Proceedings of 7th Transport Research Arena TRA 2018, April 16-19, 2018, Vienna, Austria

Electromagnetic modelling strategies for virtual testing of electrical powertrains

Alastair R. Ruddle*, Jiaqi Chen, Yu Xian Teo

HORIBA MIRA Limited, Watling Street, Nuneaton, CV10 0TU, UK

Abstract

Electrification of vehicle powertrains is a common response to societal and legislative pressures to de-carbonize transportation. Hybrid and electric cars are among the best known examples, but similar trends are also found in the marine and aerospace sectors. Electrical powertrain components are routinely optimized to meet a wide range of performance targets (electro-chemical, mechanical, thermal etc.), but there are also electromagnetic aspects to be addressed. This paper outlines strategies that have been developed for electromagnetic modelling of both electromagnetic compatibility (EMC) issues and human exposure to electromagnetic fields (EMF) associated with electrical powertrains. For EMC investigations, more practicable measurement of individual cells has been used to develop efficient hybrid 3D/circuit models for assemblies of large numbers of such cells used to form traction batteries. For EMF assessments, knowledge of the 3D geometry and the frequency content of traction current waveforms can be used to estimate the spatial distributions of low frequency magnetic fields and exposure metrics.

Keywords: automotive; computational electromagnetics; electromagnetic compatibility; electromagnetic field; traction battery.

* Corresponding author. Tel.: +44-247-635-5551; fax: +44-247-635-8551.
E-mail address: alastair.ruddle@horiba–mira.com

1. Introduction

Electrification of vehicle powertrains has become a common response to societal and legislative pressures to de-carbonize transportation. Hybrid and electric cars are among the best known examples, but similar trends are also found in the marine and aerospace sectors. Electrical powertrain components are routinely optimized to meet a wide range of performance targets (electro-chemical, mechanical, thermal etc.), but there are also electromagnetic aspects that need to be addressed. These include potential impacts on the electromagnetic compatibility (EMC) performance of the vehicle platform, as well as human exposure to the associated electromagnetic fields (EMF).

With regard to EMF, the fluctuating traction current waveforms on the high voltage (HV) power network give rise to low frequency (<2 kHz) magnetic fields. Such fields may represent a potential threat in terms of electro-stimulation of nerves and muscle, which is a well-established physiological effect. Limits for human exposure to EMF have therefore been recommended by various international organizations, including the European Union (EU, 1999; EU, 2013) and the International Commission for Non-ionising Radiation Protection (ICNIRP, 1998; ICNIRP 2010). Consequently, a new IEC standard PT 62764–1 relating specifically to the measurement of low frequency magnetic field exposure in the automotive environment is currently under development (IEC, 2017).

For EMC, however, the much higher frequency (100 kHz to 200 MHz) properties of traction battery systems determine the propagation of conducted electromagnetic emissions on the HV power network. These emissions originate from switching devices in systems such as inverters and DC–DC converters, but the traction battery system nonetheless forms a significant part of the conducting path. A further consideration is the potential for radio-frequency (RF) electromagnetic coupling between the HV power network and the low voltage (LV) wiring that also permeates traction battery systems, supporting essential battery monitoring and control functions. The latest edition of the CISPR 25 standard for automotive sub-system EMC (CISPR, 2016) therefore now includes limits and test methods for RF HV–LV coupling in HV automotive sub-systems, including traction batteries.

Numerical simulation of these issues is important for a number of reasons. Mitigation measures for low frequency EMF are very difficult to implement in the later stages of vehicle development, with increasing physical separation between the HV current paths and the occupants being the most effective approach. Early indications of potential issues would therefore be of significant benefit to vehicle manufacturers, and simulations also provide a low-cost and convenient approach for evaluating potential mitigation measures. Furthermore, if the resulting field environment is sufficiently high that induced in-body field levels need to be investigated then numerical simulation is the most practicable option. In addition, the high frequency impedance characteristics of traction batteries are not easy to measure, as suitable instruments (e.g. vector network analysers) must be protected from the high operating voltages (batteries operating at >600 V DC are already found in cars). Furthermore, working on HV systems is potentially hazardous.

This paper outlines strategies that have been developed for electromagnetic modelling of both EMF and EMC issues in electrical powertrains. For EMC investigations, more practicable measurement of individual cells has been used to develop efficient hybrid 3D/circuit models for assemblies of large numbers of such cells used to form traction batteries. The computed impedance properties can then be exploited in circuit simulations. For EMF assessments, knowledge of the 3D path geometry and frequency content of traction currents can be used to estimate the spatial distributions of low frequency magnetic fields.

2. Traction Battery Construction

Automotive traction batteries are implemented as assemblies of potentially large numbers of individual cells (typically of the order of 10^1–10^3 cells, depending on the specific cell type and application requirements) that are connected together in order to achieve the required operating voltage and traction current capability. Furthermore, the cells are commonly arranged in series and parallel combinations, via internal bus bar structures, within intermediate “battery module” assemblies in order to facilitate easier and safer assembly and handling. A suitable number of such modules may then be connected together, using appropriately rated interconnecting bus bars, in order to implement the full battery pack. Consequently, traction batteries are normally physically large assemblies (e.g. length/width of 1–2 m or more) that are often located either below the vehicle floor or behind the rear seats.

A variety of different cell types have used for automotive traction battery applications, including prismatic, cylindrical and pouch cells, in a wide variety of electro-chemistries. However, cylindrical lithium ion cells in

18650 format (i.e. approximately 18 mm in diameter and 65 mm long) offer cost, availability, sourcing and packaging flexibility advantages that are of particular interest for vehicle applications, where space is heavily constrained and production is highly cost sensitive. Hence, this type of cell is already used in Tesla electric cars.

In order to ensure safe operation it is also necessary to include monitoring and control functions within the battery assembly and its subsidiary modules. Parameters such as cell/module voltage and temperature are monitored, as well as the temperature and flow rate of coolant, since most systems require cooling. The HV switchgear that is used to connect the traction battery to the other HV electrical powertrain components (i.e. inverters etc.) also requires suitable control and monitoring. Thus, the traction battery is generally connected to a suitable cooling circuit as well as to the vehicle's LV power and data networks. The latter typically use a CAN (controller area network) protocol. In addition, a manual mechanical switch is included in the bus bar network in order to provide a means for safe isolation of the traction battery for maintenance and in the event of an emergency.

3. Characterization of 18650 Cylindrical Cells

The cells used to construct tractions batteries contain intricate internal structures with dimensions down to µm and materials with RF electrical properties that are probably unknown and difficult to determine. Thus, system complexity, electrical properties of materials and the wide range of physical scales that are involved make modelling the electromagnetic properties of traction battery systems a challenging task. A crucial simplification in the development of practicable electromagnetic models of batteries is therefore to use equivalent cell models that can be derived from measurements, thus avoiding the need to include the intricate internal details of the cells in a 3D model of the wider battery assembly.

Although impedance spectroscopy measurements (Barsoukov and Macdonald, 2005) are routinely carried out on battery cells, these are typically limited to frequencies <5 kHz. Higher frequency measurements on 18650 lithium ion cells have been reported (Muenzel et al., 2015), but only for frequencies up to 100 kHz, which does not reach the lowest frequency of interest for conducted EMC investigations. Impedance measurements as high as 40 MHz have been reported for a number of cells and cell assemblies using an impedance analyser (Hoene et al., 2003), but these did not include 18650 lithium ion cells, and impedance data is required up to 108 MHz for EMC purposes.

The RF impedance characteristics of automotive grade 18650 lithium ion cells have been established (Ruddle, Chen and Teo, 2017) from vector network analyser measurements on single cells inside conducting tubes from 100 kHz to 200 MHz. The sample 18650 cells were found to exhibit a small resistance and a small inductive reactance, with both rising from values of ~0.1 Ω at 100 kHz up to ~2 Ω by 200 MHz (see Fig. 1).

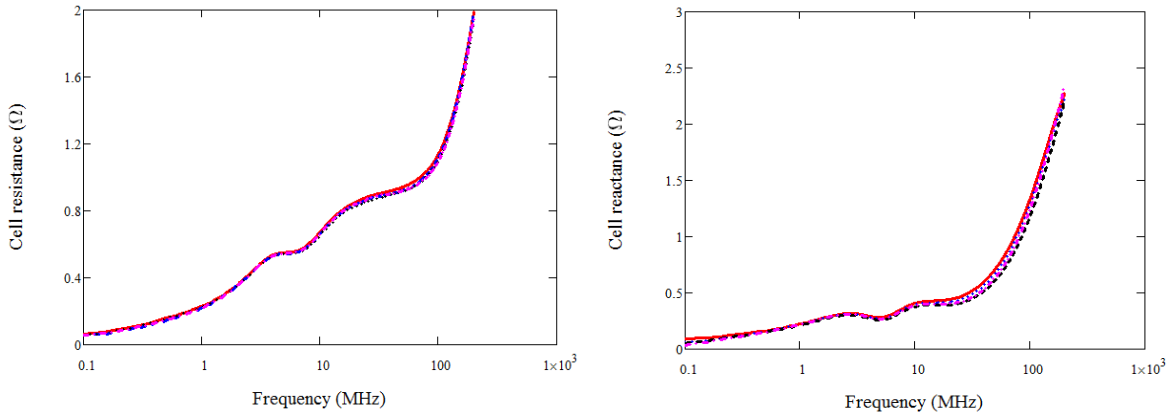

(a) 18650 cell resistance *(b) 18650 cell reactance*

Fig. 1 Impedance characteristics of sample 18650 cells derived from four measurements – carried out on two sample cells using test fixtures with two different diameters: (a) resistance; (b) inductance

A behavioural model was derived from these results, which comprises a simple 3D structure that represents the external electromagnetic interactions, coupled with a lumped element equivalent circuit representing the internal impedance between the electrodes. The measured system is outlined in Fig. 2(a), for which the reflection coefficient at the reference plane denoted *A* was measured using a vector network analyser. For the 18650 cells that were investigated the outer can is connected to the negative electrode of the cell, which is insulated from the

small disk that provides the positive contact at one end. The estimated external inductance of the cells inside the tubes was found to correspond to a current flowing on a hypothetical cylinder with a diameter that is slightly smaller than the inner diameter of the cell case (Ruddle, Chen and Teo, 2017). This suggested a 3D element for the hybrid cell model that comprises a solid cylinder surrounded by a coaxial shield that is open at the positive electrode end as illustrated in Fig. 2(b), both with perfect electrical conductor properties. This hybrid model was then validated through measurements and simulations of two such cells in series (Chen, Ruddle and Teo, 2017).

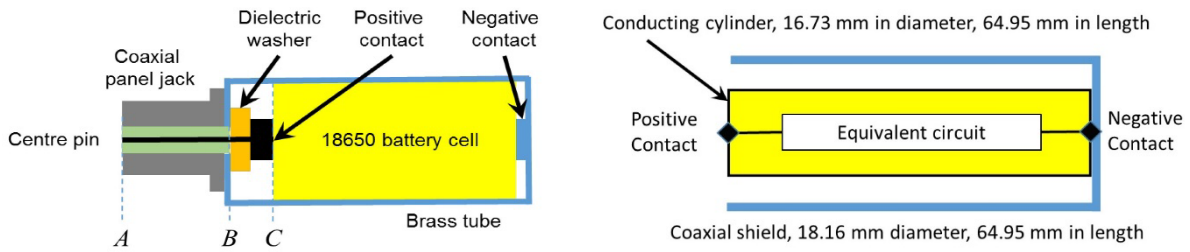

(a) Measurement system *(b) Behavioural cell model*

Fig. 2 Cell characterization: (a) cylindrical cell measurement system; (b) equivalent behavioural model

Further investigations (Chen, Ruddle and Teo, 2017) indicated that the 3D element of the cell model could be further simplified to a simple conducting cylinder (i.e. omitting the coaxial shield) for the case where the surrounding tube was about 4 mm distant. This simplified representation for the 18650 cells provides a basis for building electromagnetic models of more complex multi-cell assemblies for the analysis of both EMC and EMF issues.

4. EMC Analysis (0.1–200 MHz)

Due to electrical safety considerations automotive HV sub-systems are generally housed in conducting enclosures, and shielded cables are normally used to implement the HV power network that connects the HV sub-systems together to form the electrical powertrain. This shielded arrangement allows the HV subsystems, and their interconnecting cables, to be considered as discrete elements that are connected at well-defined “ports”. Consequently, the conducted RF propagation characteristics of the cables and other subsystems, including the traction battery assembly, can be described in terms of their scattering matrices. Cascading the individual scattering matrices in the appropriate order thereby allows the properties of the overall system to be described.

In many traction battery designs the intermediate battery modules are themselves housed within their own conducting enclosures, thereby allowing the scattering matrix formalism to be adopted at module level within the battery assembly. In order to investigate strategies for the modelling of larger scale systems, simulations of a representative battery module assembly have been carried out (Ruddle, Teo and Chen, 2017) using CST Microwave Studio (CST, 2017). Full wave solvers operating in both the time domain (finite integration technique – FIT, with hexahedral meshing) and the frequency domain (finite element method – FEM, with tetrahedral meshing) were used, for mutual validation purposes.

The assembly under investigation, which is illustrated in Fig. 3(a), can accommodate 99 cylindrical 18650 cells connected in parallel between a pair of planar internal copper bus bars. A cell carrier, made from dielectric with a relative permittivity of 3.4, locates the cells between the internal bus bars. Other dielectric parts, which are made from a material with a relative permittivity of 3.5, are included to ensure that the module terminals and internal bus bars are isolated from the aluminium case that encloses the module. In practice the module case would ultimately be electrically bonded to the shielded enclosure of a full traction battery pack.

For hybrid simulation of the 3D and circuit elements of the model in CST Design Studio (CST, 2017) internal ports are required in order to link the 3D and circuit models. For simulation purposes the module was populated with only 33 cells, located around the periphery of the cell carrier where the internal bus bars are in closest proximity to the cells as outlined in Fig. 3(b), in order to limit the computing requirements and the complexity of the models. Using only 33 cells limited the number of internal ports needed to connect to the equivalent circuits (representing the internal RF impedance properties of the 18650 lithium ion cells) to only 66, rather than the 198 that would be needed for the fully populated module.

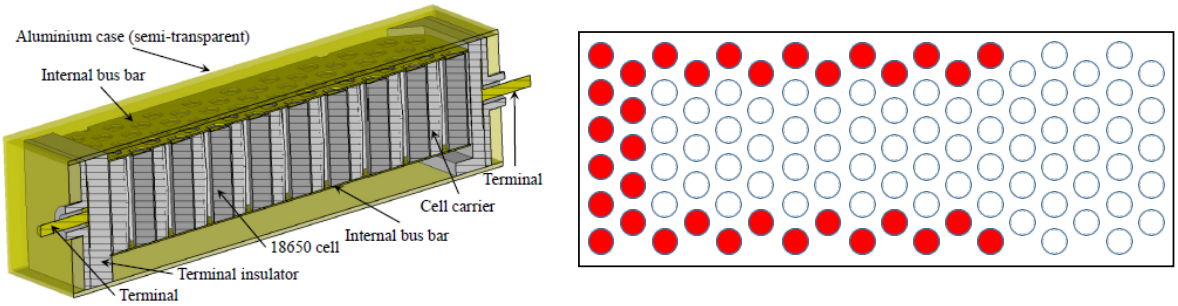

(a) Module assembly vertical cut-plane through longitudinal axis

(b) Occupied cell locations (shaded circles) for reduced model with only 33 out of 99 cells included

Fig. 3 Representative module used for analysis: (a) cut-away view of design; (b) partial population scheme

External ports were defined between the module terminals and the enclosure to enable simulation of the two-port scattering matrix, from which the impedance matrix [$\mathbf{Z}(f)$] can be derived. For a reciprocal system it can be shown (for a "π" network) that the impedance $Z_{TT}(f)$ between the terminals is (Ramo, Whinnery and van Duzer, 1994):

$$Z_{TT}(f) = \frac{Z_{11}(f)Z_{22}(f)}{Z_{12}(f)} - Z_{12}(f) \tag{1}$$

For the FEM simulations, surface ports were used to place the equivalent circuit element of the cell behavioural model at the centre of each cell. For the FIT simulations, surface ports are not available and the equivalent circuit was implemented using wire ports that were located at the positive terminal of each of the cells, with the cylinders slightly shortened to allow this.

Initial baseline models were constructed to include all of the module structures shown in Fig. 3(a), together with 33 instances of the cell model as indicated in Figure 3(b). The magnitudes of $Z_{TT}(f)$ obtained from FEM and FIT for these full model cases are very similar, as illustrated in Fig. 4(a), although the resonant frequencies differ by ~7%. The impedances of the individual cells are small, and in the module the effective impedance presented by an array of cells between the internal bus bars will be much reduced due to the large number of such cells in parallel. Further models of increasing simplicity were derived from the full models by progressively removing the cell equivalent circuits, the internal ports, the cell coaxial shields, the dielectric cell carrier, and the terminal insulators. As the difference in the resonant frequency persists in the simpler models, which do not use the different internal ports, this perhaps originates from differences in meshing between FIT and FEM. Comparing the simplified models with the baseline models:

- Removing the equivalent circuits from the internal ports gave virtually identical results to the full model cases, confirming that the impact of the individual cell impedances are negligible for the module as a whole. For a fully populated module with 99 cells in parallel the effective impedance presented by the cells would be even smaller.

- Eliminating the internal ports, which are not necessary when there is no need to include the circuits representing the internal impedances of the cells, made negligible difference for the FIT models, and resulted in a resonance shift of only 1% for the FEM models.

- For the module design studied in this work the smallest distance between the coaxial shield of the cell, which is connected to the negative cell terminal, and the positive bus bar is around 3.57 mm. Earlier studies (Chen, Ruddle and Teo, 2017) suggested that the shield would have little impact at a separation of this order. Simulations without the shield confirmed these expectations, with the simplified models giving almost identical results at considerably reduced memory and run-time (see Table 1).

- Simulations carried out with and without the dielectric cell carrier included demonstrate that this structure also has negligible impact on the impedance characteristics. However, omitting this component has a significant impact on the number of mesh elements that are required, and hence on the model computing requirements, most notably for the tetrahedral FEM models where the memory requirement is reduced by more than 50% (see Table 1).

- Although dielectric properties of the terminal insulator material are very similar to those of the cell carrier, the fields are expected to be more intense in the vicinity of the terminals than for the region in close proximity to the 18650 cells. Changes in the magnitudes of the resulting computed impedances $Z_{TT}(f)$ are illustrated in Fig. 4(b), which are due to the terminal insulators. The FIT and FEM results for $|Z_{TT}(f)|$ are again very similar (apart from the previously noted difference in the resonance), with both showing a consistent increase of 4.5% in the resonant frequencies due to neglecting the terminal insulators. Consequently, this simplification step does introduce clear changes that might be undesirable.

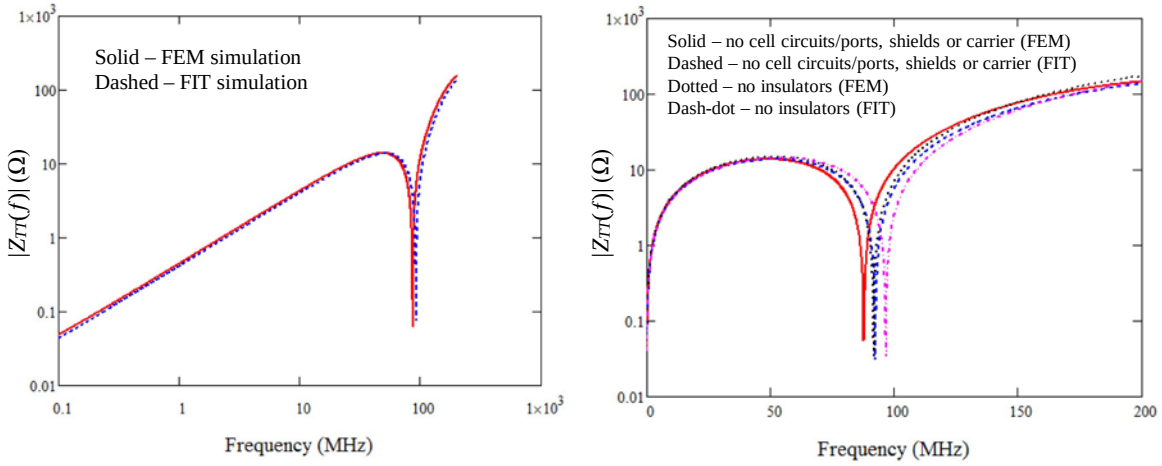

(a) Baseline models *(b) Impact of terminal insulators*

Fig. 4 Results of FEM and FIT simulations of partially populated modules: (a) comparing baseline (full) module models; (b) illustrating impact of omitting terminal insulators from simplified models

For both solvers, the greatest time saving was achieved by removing the internal ports and cell equivalent circuits (see Table 1). Simplifying the 3D geometry gave more modest benefits in terms of run-time, but provided substantial reductions (>50%) in the memory (RAM). These results indicate the significant computational savings that can be achieved by using the simplified models, with negligible impact on the predicted results. Furthermore, the similarities between the FEM and FIT models give confidence that the time domain models, which are more efficient in terms of time and memory, are suitable for building practicable models of larger scale cell assemblies representing larger modules (e.g. module illustrated in Fig. 5) as well as complete traction battery assemblies.

Table 1. Computing requirements for FIT and FEM model variants representing partially populated battery module.

	FIT models			FEM models		
Model content	Hexahedra (1000s)	RAM (Gbytes)	Time (hours)	Tetrahedra (1000s)	RAM (Gbytes)	Time (hours)
Full model with cell circuits, shields etc.	5154	5	19.58	693	55	18.75
Model with ports and cell circuits omitted	5075	5.1	0.68	594	45	1.57
Model with no cell circuits or shields	3465	3.5	0.37	546	39	1.38
Cell circuit, shield, and carrier omitted	2703	2.3	0.25	348	18	0.7

The module design studied in this work is housed in a conducting enclosure. For EMC analysis, a battery pack formed by linking a number of such modules can therefore be approximated by integrating the scattering matrices for the modules into a 3D model representing the interconnecting bus bars to complete the HV network, as well as the surrounding battery pack enclosure and the internal LV cabling. The module scattering matrices could be obtained directly from measurements at module level, or indirectly from a 3D model of the module assembly that is based on the measured impedance characteristics of the constituent cells (as described above).

A model of this nature can then be used to predict the RF coupling between the HV and LV ports of the battery, as outlined in CISPR 25 (CISPR, 2016). Furthermore, information regarding the RF impedance properties and conducted noise characteristics of other HV subsystems such as inverters can be used with the electromagnetic model of the battery to assess the propagation of conducted emissions in the HV power network.

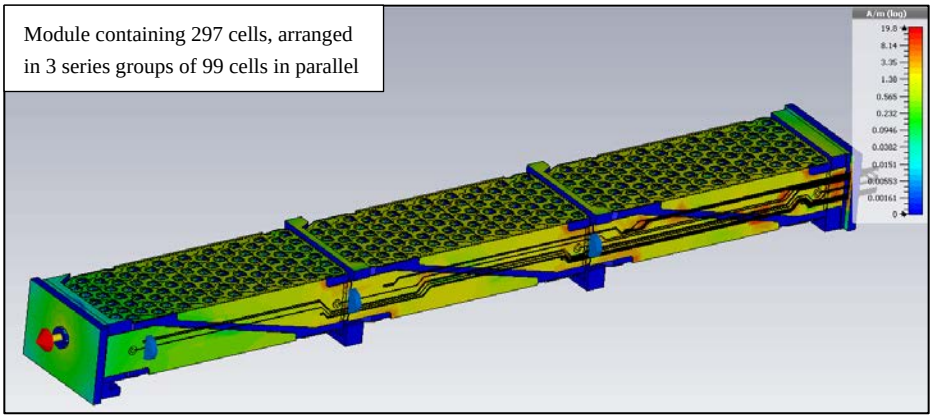

Fig. 5: Computed surface current distribution on internal bus bars of module with flexible printed interconnects (module enclosure hidden from view)

However, for designs that do not use subsidiary modules, or which do not employ conducting enclosures for the modules, it would be necessary to include representations of all of the cells in a single 3D electromagnetic model. Although the individual cells could still be represented using equivalent models derived from the measured impedance characteristics of sample cells, an electromagnetic model with this level of complexity would present a much more significant computational challenge than the approach outlined above.

5. EMF Analysis (1–2000 Hz)

The need to assess the possible exposure of vehicle occupants to low frequency magnetic fields is an emerging vehicle design requirement (IEC, 2017) that is of particular significance for hybrid and electric vehicles. The rapidly changing magnetic fields that are associated with HV traction currents induce electric fields that drive currents in weakly conducting biological tissues, with potential for electro-stimulation of the peripheral and central nervous systems at frequencies from 1 Hz to 10 MHz (EU, 1999; EU, 2013; ICNIRP, 2010). This is one of a number of well-established physiological phenomena associated with exposure to electromagnetic fields, which also include tissue heating and contact currents at higher frequencies. Various national and international bodies have therefore recommended limits for human exposure to such fields in order to avoid the potential adverse effects of these phenomena. Examples include the European Union's recommendation 1999/519/EC for general public exposure to electromagnetic fields (EU, 1999) and more recent directive 2013/35/EU concerning occupational field exposure (EU, 2013), which are based on the ICNIRP recommendations (ICNIRP, 1998; ICNIRP, 2010).

A common feature of in-vehicle magnetic field measurements (Schmid, Überbacher, and Göth, 2009; Ruddle, Low, and Vassilev, 2013) is that the highest fields tend to be found where the body is close to HV power cables (often near the feet of the driver or front passenger) or traction batteries (e.g. around the lower back for rear passengers in vehicles with batteries located in the rear). Batteries are sometimes also mounted below the occupants in some vehicle architectures, while the electric motors are generally located at the front and/or rear axles. The interconnecting HV power cables may carry current in single-phase or three-phase form, depending on whether the inverters are located with the motors, or with the battery. The traction battery typically contains an extended HV current path and is therefore a significant contributor to occupant exposure to in-vehicle magnetic fields.

The magnetic field exposures resulting from traction current transients have been found (Ruddle, Low, and Vassilev, 2013) to be both time-varying (with temporal gradients of >100 μT/s) and spatially non-uniform (with spatial gradients of >100 μT/m). Consequently, for a magnetic flux density $\mathbf{B}(t_u,\mathbf{r}_j)$ at point $\mathbf{r}_j$ and time t_u the net exposure at each point in space and time, should satisfy the criterion:

$$\sqrt{\sum_{k=1}^{3}\left[be_k\left(t_u,\mathbf{r}_j\right)\right]^2} < 1 \tag{2}$$

where the terms $be_k(t_u,\mathbf{r}_j)$ represent time-varying magnetic field exposure measures, determined for each of the Cartesian components k (where $k\in\{1,2,3\}$) of $\mathbf{B}(t_u,\mathbf{r}_j)$, which are evaluated (ICNIRP, 2010) as:

$$be_k\left(t_u,\mathbf{r}_j\right)=\sum_{n=N}^{P}\left|\frac{B_{j,k,n}}{\sqrt{2}B_L\left(n\Delta\right)}\cos\left\{2\pi n\Delta t_u+\arg\left(B_{j,k,n}\right)+\phi_B\left(n\Delta\right)\right\}\right| \tag{3}$$

In equation (3) the terms B_{jkn} represent the nth of $M/2$ complex Fourier components obtained from M+1 time samples of the magnetic flux density waveform $B_{jk}(t_u,\mathbf{r}_j)$ for Cartesian component k at point $\mathbf{r}_j$ and time t_u (for $0\leq u\leq M+1$) and Δ is the corresponding frequency increment, while $N\Delta\geq 1$ and $P\Delta\leq 10^7$ such that the summation is limited to the band from 1 Hz to 10 MHz in the ICNIRP and EU documents. The field reference level $B_L(n\Delta)$ for magnetic flux density is specified as an RMS value in the ICNIRP and EU documents, and is therefore multiplied by $\sqrt{2}$ in (3) in order to derive the corresponding peak value for comparison with the magnitudes of the spectral components ($|B_{jkn}|$). The basic restriction terms $B_L(n\Delta)$ may represent either general public or occupational field exposure reference levels, as required.

Considering the frequency response of the basic restrictions as a filter function, the parameters $\phi_B(n\Delta)$ are the phase angles of the filter, which vary according to the frequency dependence of the particular reference level or basic restriction that is used. The filter phase angles are specified (ICNIRP, 2010) as π, $\pi/2$, 0 and $-\pi/2$ radians where the frequency dependence of the basic restriction varies as f^{-2}, f^{-1}, f^0 and f, respectively.

The time-varying magnetic flux density distribution $\mathbf{B}(t_u,\mathbf{r}_j)$ that is associated with the traction current, can be predicted from knowledge of the 3D current paths and the traction current waveform. Assuming the (complex) current spectrum I_n for frequencies $n\Delta$ (where n is an integer $0\leq n\leq M/2$) to be derived from M+1 time samples with a corresponding frequency increment Δ, the magnetic flux density waveform $B_k(t_u,\mathbf{r}_j)$ for field component k at observation point $\mathbf{r}_j$ and time t_u (where $0\leq u\leq M$) is estimated from the inverse Fourier transform as:

$$B_k\left(t_u,\mathbf{r}_j\right)=\frac{1}{2}C_{k,0}\left(\mathbf{r}_j\right)\left|I_0\right|+\sum_{n=1}^{M/2}C_{k,n}\left(\mathbf{r}_j\right)\left|I_n\right|\cos\left\{2\pi n\Delta t_u+\arg\left(I_n\right)\right\} \tag{4}$$

where the terms $C_{k,n}(\mathbf{r}_j)$ represent transfer functions relating a 1 A current at frequency $n\Delta$ to component k of the resulting magnetic flux density at point $\mathbf{r}_j$. The corresponding computed magnetic field exposure measure $ce_k(t_u,\mathbf{r}_j)$ for component k can then be derived in a similar manner to (3), using:

$$ce_k\left(t_u,\mathbf{r}_j\right)=\left|\sum_{n=N}^{P}\frac{C_{k,n}\left(\mathbf{r}_j\right)\left|I_n\right|}{\sqrt{2}B_L\left(n\Delta\right)}\cos\left\{2\pi n\Delta t_u+\arg\left(I_n\right)+\phi_B\left(n\Delta\right)\right\}\right| \tag{5}$$

The transfer functions $C_{k,n}(\mathbf{r}_j)$ can be predicted at the design stage from knowledge of the relative geometry of the anticipated current paths, the expected occupant locations, and the geometry and electrical properties of surrounding materials. This is important since metallic shields such as cable shields and vehicle body panels (even those with significant permeability as well as electrical conductivity, such as steel) are often poor or even ineffective at very low frequencies. Nonetheless, significant reductions in exposure can be achieved by measures such as increasing physical separation between the occupants and the traction current paths, or by minimising the area of traction current loops, both of which are difficult to implement in the later stages of vehicle development when prototypes become available for test. These aspects are becoming increasingly important as many electric vehicle designs employ lightweight (often non-conducting) materials and physically compact geometries in order to maximize the distance that can be travelled without recharging the traction battery.

Investigation of the magnetic flux density distribution created by the representative battery module has been carried out using the Flux3D magneto-quasistatic finite element solver (CEDRAT, 2017). As with the EMC-related investigations, Fig. 6(a) shows that the internal cell impedances have negligible impact on the magnetic field generated by a partially populated module assembly. A further potential simplification in simulations of this type is to replace the conducting cylinders representing the cells by “non-meshed coils”, which simplifies the meshing and thereby reduces the computational requirements. However, the models indicate significant proximity effects amongst the peripheral cells, as shown in Fig. 6(b), and between these cells and the internal bus bars. Consequently, non-meshed coils, which impose a uniform current distribution over their specified cross-section, are not appropriate for representing the peripheral cells (see Fig. 7). Nonetheless, this simplification is a reasonable approximation for the 49 inner cells of the fully populated module, with the 50 peripheral cells represented using meshed conducting cylinders (see Figs. 8–9).

In order to estimate the occupant magnetic field exposure associated with the electrical powertrain, the magnetic field contributions from all parts of the HV power network, but primarily from the HV cables and the HV current paths through the traction battery, should be appropriately combined at observation points that are representative of the occupant locations. Knowledge of the traction current waveform can then be used to determine whether the resulting time-varying magnetic field exposure complies with the criterion represented in equation (2).

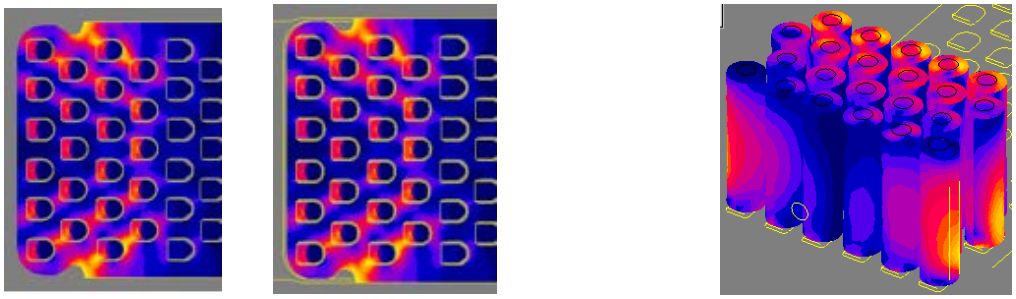

(a) With (left) and without (right) equivalent circuits *(b) Proximity effects modify cell current distributions*

Fig. 6 Computed surface currents for partially populated module at 2 kHz: (a) on internal bus bar with and without cell equivalent circuits, shown with identical colour scales; (b) proximity effects on conducting cylinders representing cells

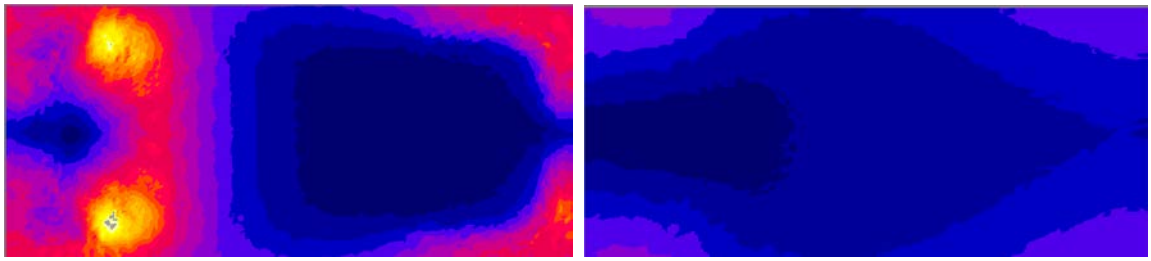

(a) All cells represented using meshed cylinders *(b) All cells represented using non-meshed coils*

Fig. 7 Magnetic flux density distribution over a horizontal plane at 4 mm above enclosure of module populated with 22 cells, shown with identical colour scales: (a) all cells represented using meshed conducting cylinders; (b) all cells represented using non-meshed coils

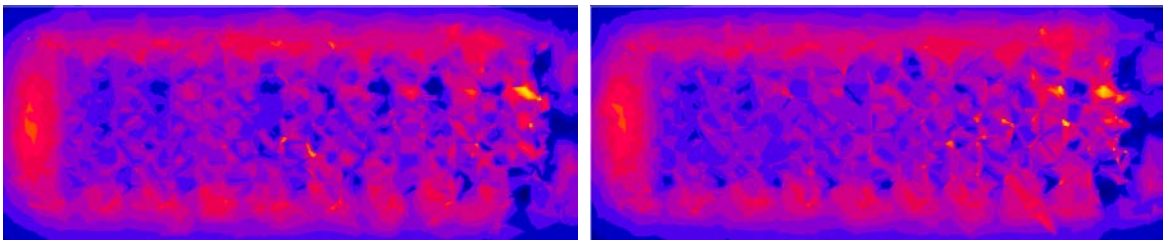

(a) All 99 cells represented using meshed cylinders *(b) Non-meshed coils representing 49 inner cells*

Fig. 8 Magnetic flux density distribution over a horizontal plane at 4 mm above enclosure of fully populated module, shown with identical colour scales: (a) all 99 cells represented using meshed conducting cylinders; (b) 49 inner cells represented using non-meshed coils

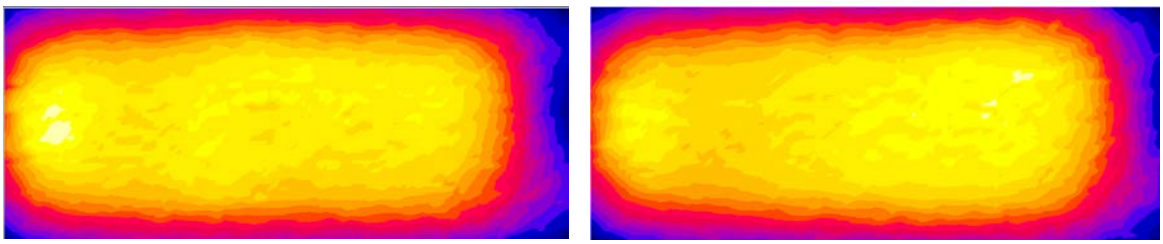

(a) All 99 cells represented using meshed cylinders *(b) Non-meshed coils representing 49 inner cells*

Fig. 9 Magnetic flux density distribution over a horizontal plane at 40 mm above enclosure of fully populated module, shown with identical colour scales: (a) all 99 cells represented using meshed conducting cylinders; (b) 49 inner cells represented using non-meshed coils

6. Conclusions

Prediction of the electromagnetic performance characteristics of automotive traction batteries is an important capability as it enables the identification and analysis of potential conducted EMC and low frequency EMF issues during the early stages of vehicle development, when mitigation strategies are considerably easier to assess and less costly to implement.

Measurement of the RF impedance of individual cells, illustrated here for standard cylindrical lithium ion cells in 18650 format, provides a basic building block for assembling larger scale electromagnetic models of multi-cell assemblies, including intermediate modules and complete battery packs. A number of approximation approaches that enable the development of practicable electromagnetic models of automotive traction batteries have been outlined, based on the measured RF impedance characteristics of commonly used 18650 lithium ion cells and illustrated using a representative module that accommodates a significant number of such cells.

Magnetic field contributions from the HV current paths through the traction battery are also important contributors to the low frequency magnetic field exposure levels for vehicle occupants. Consequently, strategies for simplifying models for the low frequency magnetic field from 18650 lithium ion cell assemblies have also been presented.

Acknowledgements

The research leading to these results was carried out in connection with the AMPLIFII project, supported in part by the UK Government's innovation agency Innovate UK (project reference 102490).

7. References

Barsoukov, E., and Macdonald, J.R. (Eds.), 2005. Impedance Spectroscopy: Theory, Experiment, and Applications. Wiley-Interscience, 2nd Edition, 2005.

CEDRAT, 2017. Flux Electromagnetic and Thermal Finite Elements Software. [Online, 2018: http://www.cedrat.com/software/flux/].

Chen, J., Ruddle, A.R., and Teo, Y.X., 2017. Predicting the RF impedance of cells in series for automotive traction battery application. Proceedings of International European Symposium on Electromagnetic Compatibility (EMC Europe 2017), Angers, France, September 2017.

CISPR, 2016. CISPR 25: Vehicles, boats and internal combustion engines – Radio disturbance characteristics – Limits and methods of measurement for the protection of on-board receivers. 4th Edition, Comité International Spécial des Perturbations Radioélectriques, October 2016.

CST, 2017. CST 3D Electromagnetic Simulation Software. [Online, 2018: https//www.cst.com/products].

EU, 1999. 1999/519/EC: Council Recommendation of 12th July 1999 on the limitation of exposure of the general public to electromagnetic fields (0 Hz to 300 GHz). Official Journal of the European Communities, No. L 199, pp. 59–70, 30th July 1999.

EU, 2013. 2013/35/EU: Directive 2013/35/EU of the European Parliament and of the Council of 26th June 2013 on the minimum health and safety requirements regarding the exposure of workers to the risks arising from physical agents (electromagnetic fields) (20th individual Directive within the meaning of Article 16(1) of Directive 89/391/EEC) and repealing Directive 2004/40/EC. Official Journal of the European Union, No. L 179, pp. 1–21, 29th June 2013.

Hoene, E., Saikly, R., Guttowski, S., John, W. and Reichl, H., 2003. RF-properties of automotive traction batteries. Proceedings of 2003 IEEE International Symposium on EMC, Istanbul, Turkey, pp. 425–428, May 2003.

ICNIRP, 1998. Guidelines for limiting exposure to time-varying electric and magnetic fields (up to 300 GHz). Health Physics, Vol. 74, No. 4, pp. 494–522, April 1998.

ICNIRP, 2010. Guidelines for limiting exposure to time-varying electric and magnetic fields (1 Hz to 100 kHz). Health Physics, Vol. 99, No. 6, pp. 818–836, December 2010.

IEC, 2017. IEC PT 62764–1: Measurement procedures of magnetic field levels generated by electronic and electrical equipment in the automotive environment with respect to human exposure. International Electrotechnical Commission. [Online, 2018: http://www.iec.ch/dyn/www/f?p=103:38:4185479064824:::FSP_ORG_ID,FSP_APEX_PAGE,FSP_PROJECT_ID:1303,23,20549].

Muenzel, V., et al., 2015. A comparative testing study of commercial 18650-format lithium-ion battery cells. Journal of the Electrochemical Society, Vol. 162, No. 8, pp. A1592–A1600, 2015.

Ramo, S., Whinnery, J.R., and van Duzer, T., 1994. Fields and Waves in Communication Electronics. Wiley, New York, 3rd Edition, pp. 536–541, 1994.

Ruddle, A.R., Low, L., and Vassilev, A., 2013. Evaluating low frequency magnetic field exposure from traction current transients in electric vehicles. Proceedings of 12th International European Symposium on EMC, Bruges, Belgium, pp. 78–83, September 2013.

Ruddle, A.R., Chen, J., and Teo, Y.X., 2017. Measurement of RF impedance for automotive 18650 cylindrical lithium ion cells. Proceedings of International European Symposium on Electromagnetic Compatibility (EMC Europe 2017), Angers, France, September 2017.

Ruddle, A.R., Teo, Y.X., and Chen, J., 2017. Electromagnetic modelling strategies for EMC analysis of automotive traction batteries. Proceedings of 19th International Conference on Electromagnetics in Advanced Applications (ICEAA 2017), Verona, Italy, September 2017.

Schmid, G., Überbacher, R., and Göth, P., 2009. ELF and LF magnetic field exposure in hybrid- and electric cars. Proceedings of 2009 Bio-electromagnetics Conference, Davos, Switzerland, Paper 9–3, June 2009.